



HAL
open science

Role of the Tide on the Structure of the Amazon Plume: A Numerical Modeling Approach

Valentin Ruault, Julien Jouanno, Fabien Durand, Jérôme Chanut, Rachid
Benshila

► To cite this version:

Valentin Ruault, Julien Jouanno, Fabien Durand, Jérôme Chanut, Rachid Benshila. Role of the Tide on the Structure of the Amazon Plume: A Numerical Modeling Approach. *Journal of Geophysical Research. Oceans*, 2020, 125, 10.1029/2019JC015495 . insu-03671102

HAL Id: insu-03671102

<https://insu.hal.science/insu-03671102>

Submitted on 18 May 2022

HAL is a multi-disciplinary open access archive for the deposit and dissemination of scientific research documents, whether they are published or not. The documents may come from teaching and research institutions in France or abroad, or from public or private research centers.

L'archive ouverte pluridisciplinaire **HAL**, est destinée au dépôt et à la diffusion de documents scientifiques de niveau recherche, publiés ou non, émanant des établissements d'enseignement et de recherche français ou étrangers, des laboratoires publics ou privés.

Copyright

Role of the Tide on the Structure of the Amazon Plume: A Numerical Modeling Approach

Valentin Ruault^{1,2}, Julien Jouanno¹ , Fabien Durand^{1,3} , Jérôme Chanut², and Rachid Benshila¹ 

¹LEGOS, IRD, Univ. Paul Sabatier, Observatoire Midi-Pyrénées, Toulouse, France, ²Mercator Ocean International, Ramonville Saint Agne, France, ³Laboratório de Geoquímica, Instituto de Geociências, Universidade de Brasília, Brasília, Brazil

Key Points:

- The sensitivity of the Amazon shelf dynamics to tidal forcing is explored with a set of high-resolution numerical simulations
- Explicit resolution of the tides significantly improves the representation of the offshore spread of the river plume
- With tides, the plume is more easily exported offshore by the North Brazil Current at the shelf break

Correspondence to:

J. Jouanno,
julien.jouanno@ird.fr

Citation:

Ruault, V., Jouanno, J., Durand, F., Chanut, J., & Benshila, R. (2020). Role of the tide on the structure of the Amazon plume: A numerical modeling approach. *Journal of Geophysical Research: Oceans*, 125, e2019JC015495. <https://doi.org/10.1029/2019JC015495>

Received 16 JUL 2019

Accepted 28 JAN 2020

Accepted article online 03 FEB 2020

Abstract The dynamical balance on the Amazon shelf and its implication on the properties of the Amazon River plume is not fully understood and poorly represented in global- and basin-scale ocean models. In this study, the sensitivity of the Amazon shelf dynamics to tidal forcing is explored with a set of high-resolution numerical simulations (1/36°) with and without the tide. A comparison of the simulations with sea surface salinity in situ measurements at 5°N (a location where the plume seasonally detaches from the coast and retroflects toward the east) revealed that the explicit resolution of the tide significantly improves the representation of the offshore spread of the river plume. This study further highlights the finding that tidal currents affect the properties of the whole Amazon plume. This sensitivity is explained by a near total collapse of the northwestward alongshore mean flow located near the river mouth, once the tidal forcing is included. This weakening of the ambient flow reduces (i) the dilution ratio between the ambient salty shelf waters and the riverine freshwaters and (ii) the constraint on the cross-shore extension of the low-salinity bulge. With tides, the plume is fresher near the river mouth (by up to 5 units), more extended in the cross-shore direction, and more easily exported offshore by the North Brazil Current at the shelf break.

1. Introduction

The Amazon River is the largest source of continental freshwater to the world ocean, with a yearly mean volume of 5,600 km³; it has a sensible seasonal variability, ranging between 250,000 m³ s⁻¹ in May and 80,000 m³ s⁻¹ in November (HYBAM, 2018). The mouth delivers the freshwater to a shallow, broad shelf, under macrotidal regime, with tidal flow ranging from 0.5 to 2.0 m s⁻¹, respectively, in ebb flow of a neap tide and in flood flow of a spring tide (Geyer et al., 1991; Geyer & Kineke, 1995). The discharge is so powerful that it consistently prevents the oceanic saltwater to penetrate in the estuary (Gibbs, 1970). Another peculiarity of the Amazon outflow consists in its location right at the equator (Figure 1a), where the effects of Earth rotation vanish. As we shall see, this peculiarity has some implications on the dynamics of the plume waters. At the shelf break the plume interacts with the North Brazil Current, a powerful western boundary current that flows northwestward and that is present in all seasons, with typical velocity of about 1 m s⁻¹ along the north coast of South America (Bourlès et al., 1999; Johns et al., 1998). The offshore export of the discharge forms a very large plume of low-salinity surface water (typically inferior to 35.5 units in the practical salinity scale) that extends from the equator to about 15°N and to the west of 45°W (Figure 1a), influencing the surface salinity of the western tropical Atlantic Ocean.

The oceanic impacts of the Amazon plume are twofold. First, on account of its strength, it is expected to have a sensible mass contribution to the ocean. For instance, the interannual variability of Amazon discharge, once converted into its equivalent in global mean sea level, amounts to 0.4 mm, which represents not less than 40% of the interannual variability of the globally averaged altimeter data (Durand et al., 2019). Regionally, this mass contribution may have a significant signature in the sea level and circulation, at least in the vicinity of the river mouth. From a 1/4° model, Giffard et al. (2019) shows that the Amazon contributes to regional mass redistributions with a decrease at the river mouth equivalent to 8 cm of mean sea level and increases on continental shelves of the Gulf of Mexico and Caribbean Sea equivalent to 4.5 cm of mean sea level. The second kind of impact the Amazon can have on the ocean physics is through its steric effect and in particular its halosteric contribution. Indeed, the freshwater discharged by Amazon River to the western Atlantic basin induces a massive density anomaly in the upper ocean. Giffard et al. (2019) shows that

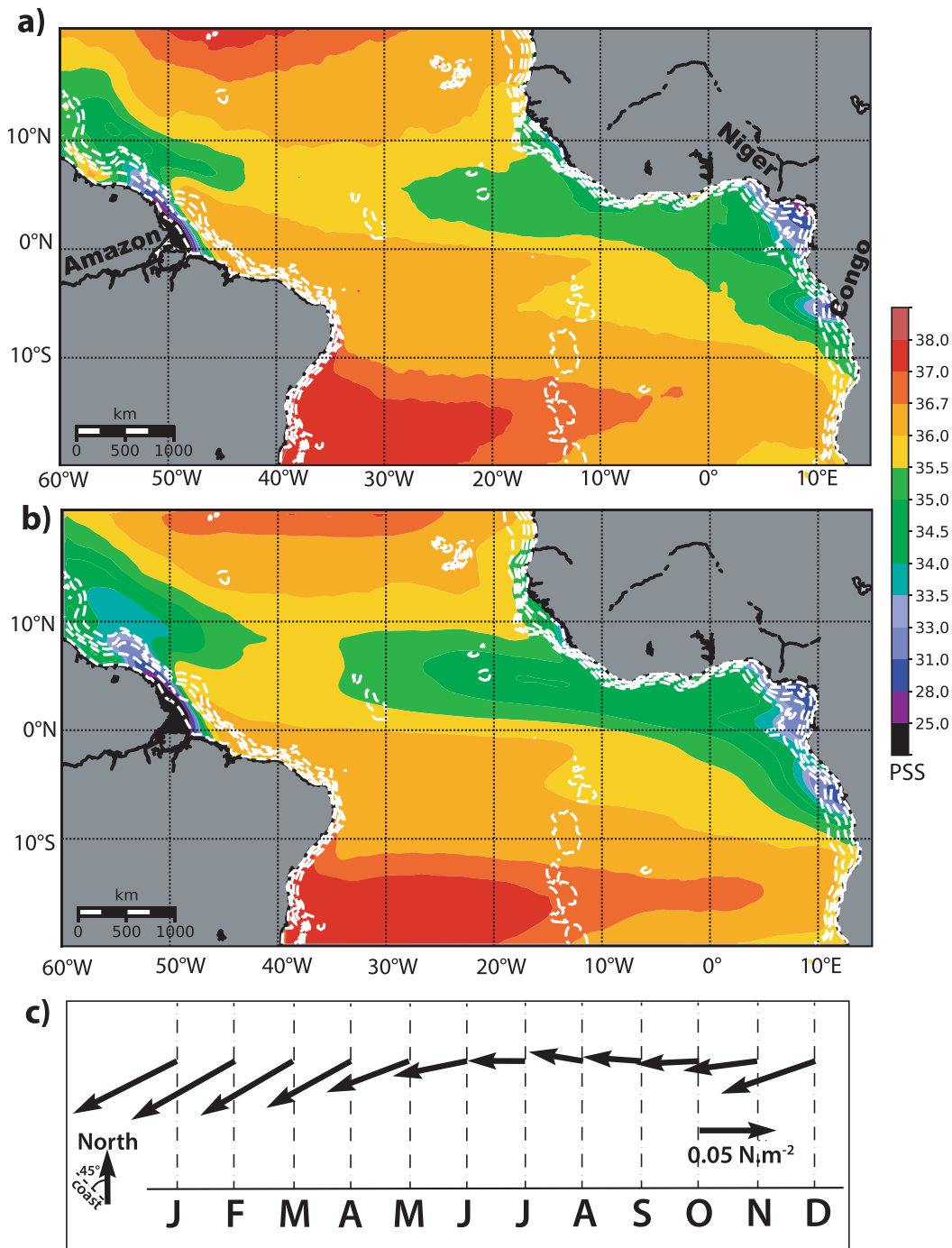


Figure 1. (a) Long-term mean SSS observed by SMAP over the tropical Atlantic basin. The locations of Amazon, Niger, and Congo Rivers are indicated. Here and in all subsequent figures, the following isobaths are shown in dashes: 3,000, 2,000, 1,000, 80, and 15 m. (b) Long-term mean SSS simulated by the model. (c) Monthly climatology of the wind stress at the mouth of the Amazon.

this halosteric effect is larger than the mass redistribution effect mentioned above, so the Amazon flow has not only a net local contribution of 10 cm to the mean state sea level at the river mouth but also a net remote contribution of 3.3 cm around the whole Caribbean Archipelago. An impact of this density anomaly on the vertical stability of the ocean, and beyond, on the regional climate of the tropical Atlantic, has been claimed in previous studies but remains controversial. Observational studies suggested that the Amazon plume

induces a vertical stability of the water column strong enough to inhibit the ocean cooling traditionally induced by tropical cyclones, hereby favoring the intensification of Atlantic hurricanes crossing the plume (Grodsky et al., 2012; Reul et al., 2014). Modeling studies, in contrast, suggest that the Amazon plume remains rather passive in the air-sea exchanges under tropical cyclones (Hernandez et al., 2016; Newinger & Toumi, 2015). Beyond the tropical Atlantic climate, the Amazon outflow is also suspected to have a profound influence on the regional continent-ocean-atmosphere water cycle and on the Atlantic climate as a whole (Jahfer et al., 2017).

In the general case, the dispersal of river plumes is driven by a variety of processes (Horner-Devine et al., 2015): the ambient coastal circulation, the stratified-flow instabilities, the buoyancy flow driven by the pressure gradient at the plume front, and the wind-induced and wave-induced mixing. In addition, for the specific case of rivers outflowing in mesotidal or macrotidal regions, the tide can act as a prominent driver of plume water transport, through residual tidal currents and/or through tidal Stokes drift. For instance, this was evidenced for the particular case of the Changjiang River by Wu et al. (2011, 2014). As we saw, the Amazon outflows in a macrotidal region as well. The tidal flow can also indirectly shape a river plume, by modulating the vertical turbulence and associated mixing, both of momentum and of freshwater (Simpson, 1997). The interplay of the different mixing processes defines the resulting structure of a given plume and its spatiotemporal evolution away from the river mouth. The dynamics of the larger river plumes such as the Amazon are very rich, with intricate processes, in particular transport by the regional circulation, local forcing by the trade winds, vertical turbulent mixing, and the effect of tidal currents (Geyer et al., 1996). These processes act over a broad range of spatial and temporal scales (Durand et al., 2019; Horner-Devine et al., 2015).

The difficulty to disentangle the mechanisms that drive the plume waters dispersal, as well as their interactions, has motivated several observational studies. At the early stage of the AMASSEDS (A Multidisciplinary Amazon Shelf SEDiment Study) program, Geyer et al. (1991) identified the salient features of the Amazon plume, its temporal scales of variability, and possible factors shaping its variability. It was found that the ambient oceanic transports are largely responsible for the plume variability. They suggested that the spring-neap tidal cycle could induce a sensible modulation of the nearshore shelf circulation, with possible impact on the alongshelf flow. The exact imprint of the tidal currents on the plume extent was not known. After completion of the AMASSEDS in situ surveys, Geyer and Kineke (1995) evidenced a significant relationship between Amazon discharge and plume extent in the near-field region, with stronger discharge associated with a freshwater front located further offshore. Similarly, they evidenced a significant relationship between tidal amplitude and plume extent, with stronger tidal currents (typically during spring tides) associated with a freshwater front also located further offshore. They observed that the classical salt wedge structure, with bottom saline water separated from the upper fresh plume by a slanted halocline, is more marked during neap tides. During spring tides, conversely, the vertical stratification in the vicinity of the river mouth has disappeared, pushed offshore up to around 150 km off the mouth. The modulation of the vertical mixing induced by the spring-neap cycle of tidal velocities was proposed as an important ingredient of this apparent spring-neap modulation of the plume extent (Beardsley et al., 1995; Lentz & Limeburner, 1995). Geyer (1995) observed that during the ebb of spring tides the vertical current shear is high enough to destabilize the vertical density stratification at the plume base, according to simple scaling of stratified-shear flow instability based on an observed Richardson number.

Regarding numerical modeling, only a handful of studies have been dedicated to the dynamics of the Amazon plume dispersal, so far. The early study of Paluszkiwicz et al. (1995) evidenced the sensitivity of the Amazon plume pathway to the local wind forcing, based on a coarse-resolution circulation model. Nikiema et al. (2007) implemented a high-resolution numerical model over the mouth of the Amazon and conducted a systematic assessment of several forcing factors that can shape the plume dispersal: the wind, the ambient coastal circulation, the tide, and the discharge. They could conclude that the factor responsible for the northwestward export of the plume in all seasons is the ambient northwestward current. Coles et al. (2013) investigated the fate of the Amazon plume through a basin-scale eddy-permitting model, but they did not consider the tide in their numerical setup; as we shall see in the following, tidal forcing is indeed a prominent factor controlling the plume properties and dispersal.

Until date, besides the limited, though extremely useful, past studies mentioned above, no in-depth assessment of the impact of the tide on the evolution of Amazon fresh water has been achieved. The objective of

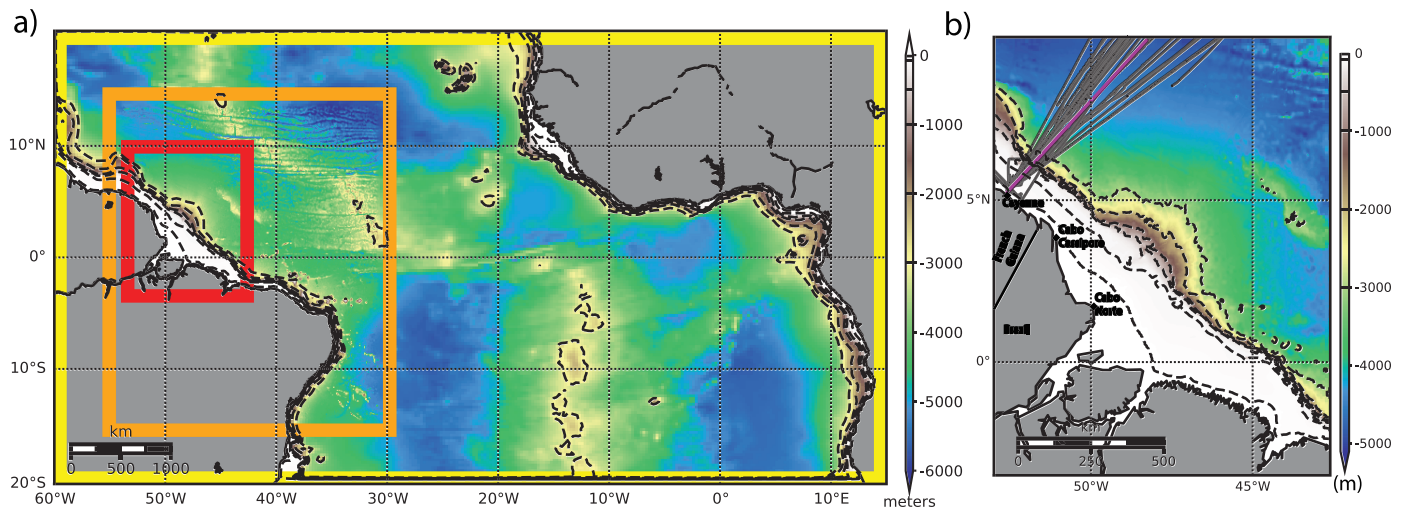


Figure 2. (a) Model bathymetry and nested computational domains. The $1/4^\circ$ domain is in yellow, the $1/12^\circ$ domain is in brown, and the $1/36^\circ$ domain is in red. (b) Location of the thermosalinograph transects used in the study (in black). The red line features the average track, along which we compute the analyzed SSS. The map extent roughly matches the finest model grid.

the present study is to assess the importance of the tide in the kinematics of the Amazon plume, through dedicated numerical modeling experiments. We make use of a general circulation model, building on the framework of Hernandez et al. (2016, 2017), but with a grid refinement strategy, focused on the Amazon mouth, that allows a cross-scale approach. The key improvement compared to that in past numerical studies is a consistent representation of the whole range of processes that are potentially important in the river freshwater export, from basin-scale circulation to fine-scale estuarine processes. As such, our study can be seen as a natural extension of the regional modeling study of Nikiema et al. (2007). More precisely, the novelty of our modeling compared to theirs concerns the three following points. First, our domain spans the whole tropical Atlantic, with a consistent dynamical link between the various forcing factors of the Amazon plume dispersal, including the large-scale circulation. Our modeling framework, in particular, accounts for the cross-shelf exchanges that have to be expected from the known active mesoscale turbulence in this western boundary region (Coles et al., 2013). This also allows us to analyze the eventual far-reaching fate of the plume, as we shall see. Second, our model horizontal resolution is twice larger than theirs in the region of interest. Indeed, a high enough horizontal resolution is a must for a realistic representation of river plumes in hydrodynamical models (e.g., Kärnä et al., 2015). Third, whereas Nikiema et al. (2007) performed short-duration model runs (typically of 400 hr long only) under idealized forcing, we considered pluriannual simulations, forced by realistic, time-varying atmospheric fluxes and river discharges, that consider the full temporal spectrum (including the seasonality) of the processes that are prone to shape the Amazon plume.

The article is organized as follows. Section 2 presents the model and the observed data sets used to validate it. Section 3 presents the validation of model sea surface salinity (SSS). In Section 4 we show the imprint of the tide on the Amazon plume pathway. Section 5 analyzes the processes responsible for this sensitivity to the tide. Section 6 is a summary and conclusion.

2. Model and Data

2.1. Model

Our model is derived from the one used in Hernandez et al. (2016, 2017). The reader is referred to these papers for full details on the model numerics. We use the NEMO 3.6 code (Madec, 2014). The model domain is displayed in Figure 2a. It covers the whole tropical Atlantic basin from 20°S to 20°N and from 60°W to the African continent. The horizontal resolution is $1/4^\circ$, and the vertical grid comprises 75 levels, 12 of which are located in the upper 20 m. The key difference between this earlier version and the one used in the present study consists in a three-level, two-way embedding of finer grids: a $1/12^\circ$ grid covering the western basin

Table 1
Characteristics of the Experiments

Simulation name	Tidal forcing	Wind forcing	Amazon River forcing	Stratification	Analysis period
Model	✓	✓	✓	✓	2005–2015
NoTIDE		✓	✓	✓	2005–2015
EXPA	✓	✓		✓	2015
EXPB		✓		✓	2015
EXPC	✓	✓			2015
EXPD		✓			2015
EXPE	✓				2015

(9 km resolution, from 15°S to 15°N, 55°W to 30°W; see brown box in Figure 2a) and a 1/36° grid (3 km resolution) covering the vicinity of the mouth of the Amazon (from 3.5°S to 10°N, from 53°W to 42.5°W; see red box in Figure 2a). All three domains share the same vertical grid and are coupled online via the AGRIF library in two-way mode (Blayo & Debreu, 1999; Debreu, 2000). This means that the model resolves much finer scales in the Amazon outflow region, ensuring a numerical consistency with the large-scale dynamics through the three nested grids. The basic idea behind this nesting is to be able to resolve with a reasonable computational cost the fine-scale processes on the Amazonian shelf (at 1/36° resolution), the western boundary dynamics including the mesoscale turbulence of the whole Amazonian plume (at 1/12° resolution), and the basin-scale tropical dynamics (at 1/4° resolution).

Temperature and salinity are advected using a flux-corrected transport scheme with nearly horizontal diffusion parameterized as a Laplacian isopycnal diffusion, with coefficients of 300, 100, and 45 m² s⁻¹ from the lower- to higher-resolution grids, respectively. A third-order upstream biased momentum advection scheme (UP3) with built-in diffusion is employed. The vertical diffusion coefficients are given by a generic length-scale scheme configured here as a $k - \epsilon$ turbulent closure. Bottom friction is quadratic with a bottom drag coefficient of 10⁻³, while at lateral walls free-slip boundary conditions are assumed. The free surface is solved using a time-splitting technique with the barotropic part of the dynamical equations integrated explicitly. A variable volume z^* vertical coordinate system is used, which relaxes the linear free surface assumption, that is, that sea level variations are small compared to the local water depth. This simplification indeed no longer stands when resolving explicitly tides on the shelf (see details in Maraldi et al., 2013).

The model is forced by DFS5.2 atmospheric fluxes (Dussin et al., 2016), which is a bias-corrected version of ERA-Interim reanalysis (Dee et al., 2011). The river discharges of Amazon and Para Rivers are injected in the 1/36° grid, based on the interannual timeseries from the HYBAM (2018) hydrological observatory, and are prescribed in the model as mass sources with null salinity through the model open boundaries at the exact location of the mouths. The other rivers flowing into the tropical Atlantic are from the monthly climatology of Dai and Trenberth (2002) and are injected in the 1/4° and 1/12° grids near the river mouths as a surface freshwater flux with increased vertical mixing in the upper 10 m (as in Hernandez et al., 2016). The model is forced by the tidal potential of all major high-frequency constituents (M2, S2, N2, K2, K1, O1, Q1, P1, and M4). At the open boundaries of the large-scale grid, we prescribe the MERCATOR GLORYS2V4 ocean reanalysis (<http://marine.copernicus.eu/documents/PUM/CMEMS-GLO-PUM-001-025.pdf>) for velocity, temperature, salinity, and sea level, along with the tidal elevation and barotropic currents of the same set of high-frequency constituents taken from the FES2012 atlas (Carrère et al., 2012). We use the General Bathymetric Chart of the Oceans (GEBCO) bathymetry (Weatherall et al., 2015) interpolated on each of the three nested grids. The period of simulation is 2000–2015, but only the period 2005 to 2015 is analyzed in this study.

The model realism in terms of regional circulation, thermal and haline structures, was assessed following the same validation procedure as in Hernandez et al. (2016, 2017), both for the long-term mean and for the seasonal variability, and it was found that the overall performance of our configuration is in line with these earlier studies. For the sake of conciseness, we do not present the full validation here, and we refer instead to these past papers. In section 3 we will specifically focus on the validation of the key variable that characterizes the Amazon plume waters: the upper-ocean salinity.

We performed various sensitivity experiments, which are summarized in Table 1. First, we performed a sensitivity experiment where we switched off the tidal forcing throughout the three model grids, as well as at the outer-domain open boundaries. This experience is referred to as NoTide and has been run for the same period as the reference simulation. We also performed five additional 2-year-long sensitivity experiments initialized from the reference simulation on 1 January 2014, which are referred to as EXPA, EXPB, EXPC, EXPD, and EXPE. In these, only year 2015 is analyzed. These short simulations have no Amazon River forcing and alternately include or not tidal forcing, wind forcing, and density stratification (Table 1). This latter results in

a barotropic experiment; this is achieved by keeping the three-dimensional temperature and salinity fields at constant values throughout the domain (28 °C and 38 units, respectively).

2.2. Soil Moisture Active Passive

The Soil Moisture Active Passive (SMAP) satellite provides measurements of SSS. It has been operating since 2015. SMAP salinity data were used in a variety of river plume environments (Fournier et al., 2016, 2017; Silva & Castela, 2018). Here we use the monthly level-3 product at a resolution of $1/4^\circ$, available from <https://podaac.jpl.nasa.gov>. SMAP long-term mean SSS displayed in Figure 1a shows the large-scale features of the tropical Atlantic basin, with salinity maxima in the core of the subtropical gyres around 15°N and 13°S and an elongated band of low SSS along the intertropical convergence zone quasi-zonally oriented around 5°N . SMAP distinctly captures the signature of the large river plumes along the coast of Africa (Niger, Congo) as well as the plume of the Amazon that forms the focus of our study.

2.3. LEGOS SSS

As SMAP resolution does not allow to capture the finer scales of the Amazon outflow, we will rely on the high-resolution in situ salinity measurements of the Service d'Observation on Sea Surface Salinity (SO-SSS) network (available from sss.sedoo.fr; DOI.10.6096/SSS-LEGOS). Over our area, these measurements consist of thermosalinograph records harvested along a repeated ship track, from vessels plying regularly between Cayenne (French Guiana; 5°N , 52.7°W) and mainland France (Figure 2b), which are collected and distributed via the French ORE-SSS salinity observation service (see more details in Alory et al., 2015). These tracks have been typically covered at bimonthly frequency, since 1993. Overall, we could analyze 74 individual transects, over 2005–2015. We considered only the measurements flagged as “good data” (quality control flag of 1 in the SO-SSS processing pipeline). So as to be consistent with the resolution of our numerical model, the various SSS transects were binned on a regular 2,400-m-resolution grid along the track displayed in pink in Figure 2b. Then, the individual transects were averaged into trimonthly climatological means, for December-January-February (DJF; 11 transects), March-April-May (MAM; 19 transects), June-July-August (JJA; 26 transects) and September-October-November (SON; 18 transects).

3. Model Validation

3.1. Large scale Sea Surface Salinity distribution

The model long-term SSS is displayed in Figure 1b. It is seen that the model successfully reproduces the observed large-scale patterns, with subtropical maxima properly located in both hemispheres. The quasi-zonal band of low SSS under the intertropical convergence zone (ITCZ) is also adequately simulated. The model is slightly biased toward low values (by about 0.5 unit) in the core of the fresh tongue (between the equator and 5°N), to the east of 30°W . The model successfully captures the signature of the three major rivers outflows (Niger, Congo, and Amazon). The Amazon plume, however, appears also too fresh in the model, with a typical offset of about 0.5 unit at the scale of the whole plume. Such values of the model SSS biases are commensurate with the biases of state-of-the-art models published in the recent years (Coles et al., 2013; Hernandez et al., 2016, 2017).

3.2. Amazon Plume Region

Since we wish to analyze the role of the tide in the Amazon plume water dispersal, it is important to assess the quality of the tide simulated in our model. Over the Amazonian shelf, most of the tidal energy is contained in M2 and S2 semidiurnal constituents (Beardsley et al., 1995). Figure 3 shows the amplitudes of the M2 and S2 constituents, obtained from the model (computed using hourly sea level from year 2015) and from the FES2012 tidal atlas (Carrère et al., 2012). Note that this comparison cannot be seen as a quantitative validation, strictly speaking, as the FES2012 atlas is used to force the model tidal dynamics at the open boundaries of our outer grid (see section 2). Rather, it should be seen as an indication of the capability of the model to propagate the tide through the three embedded levels of nests and to simulate the coastal increase of tidal amplitude over our region of interest in the inner nest, which is the Amazonian shelf. It is seen that, for both M2 and S2, the model successfully captures the local maxima seen immediately to the northwest and southeast of the Amazon outlet. The northern local maximum seen around 2°N , 50°W (between Cabo Norte and Cabo Cassipore) results from the semidiurnal frequencies being close to resonance in this embayment (Beardsley et al., 1995). The values of the maxima simulated by the model are in gross

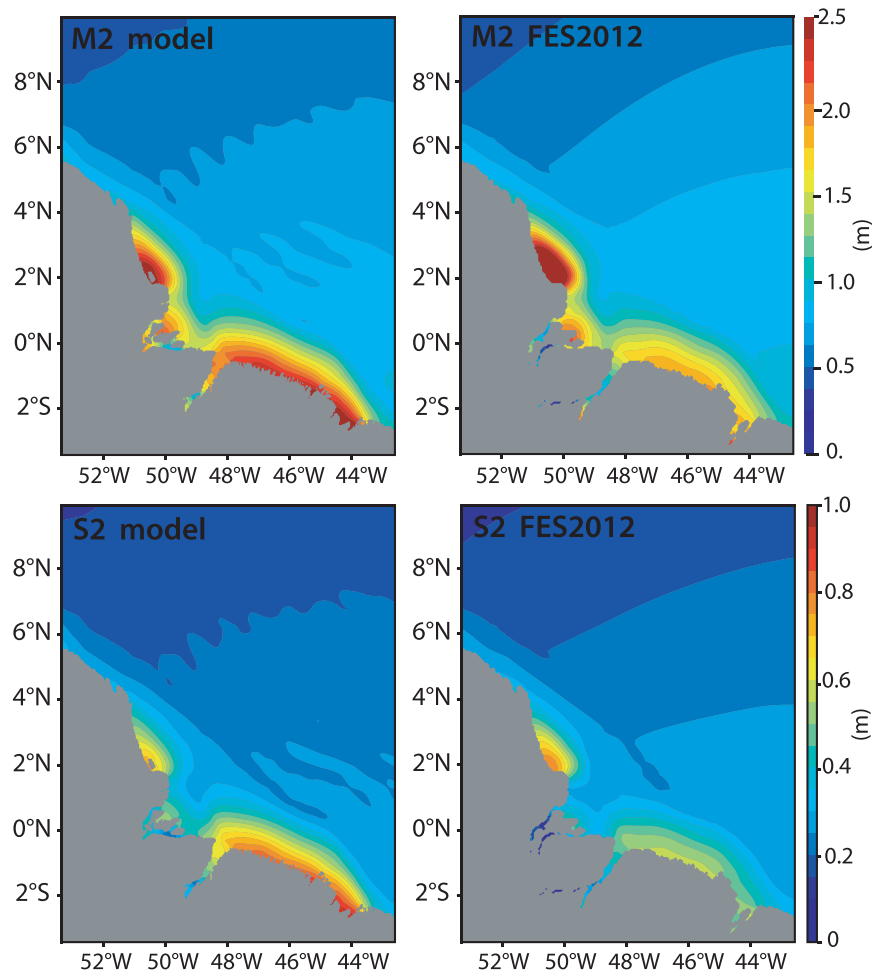


Figure 3. Amplitude of the M2 and S2 semidiurnal tidal constituents simulated by (left column) the model, compared with the (right column) FES2012 (Carrère et al., 2012) tidal atlas.

agreement with those of the tidal atlas, with mismatches of order 0.25 m (positive or negative, for M2 and S2, for the northwestern or southeastern coastal maxima, and locally reaching 0.6 m). Such an agreement is quite remarkable, given the known very strong sensitivity of the tide simulated by the models to their bathymetry over the Amazonian shelf (Le Bars et al., 2010), and keeping in mind that we did not attempt to optimize the GEBCO bathymetry used in our model. The ratio of S2 versus M2 amplitudes, of about 1/3, is consistent with the observed values reported by Beardsley et al. (1995) and implies a large spring-neap variability of the tidal flow.

In addition to the tide, SSS is also a key variable of the processes discussed in the following. Hence, we present a validation of the model SSS against the high-resolution along-ship track transect observations presented in section 2.3. Although the ship track does not intersect the plume right at the mouth of the Amazon, its proximity (500 km to the northwest of the mouth) is sufficient to capture its imprint. The plume appears in the seasonal averages of the observed salinity shown in Figure 4, with varying magnitude and position. In DJF, it has a minimum core of 30 units, very close to the shore, at 52.5°W. Following the seasonal increase of the discharge during the subsequent flood season, the core freshens to 27.5 units in MAM, still hugging the coast. Subsequently in JJA, the core of the plume is shifted 75 km offshore (at 52°W), with a similar value (28 units). Afterward, during the low-discharge SON season, the core shifts further offshore to 51.75°W and gets saltier (31 units). Note that the gradual increase in salinity between these plume core values and the offshore oceanic values, apparent in all season, is in contrast with the sharp frontal structure ubiquitous in all previous studies (e.g., Lentz & Limeburner, 1995) and simply results from the averaging we

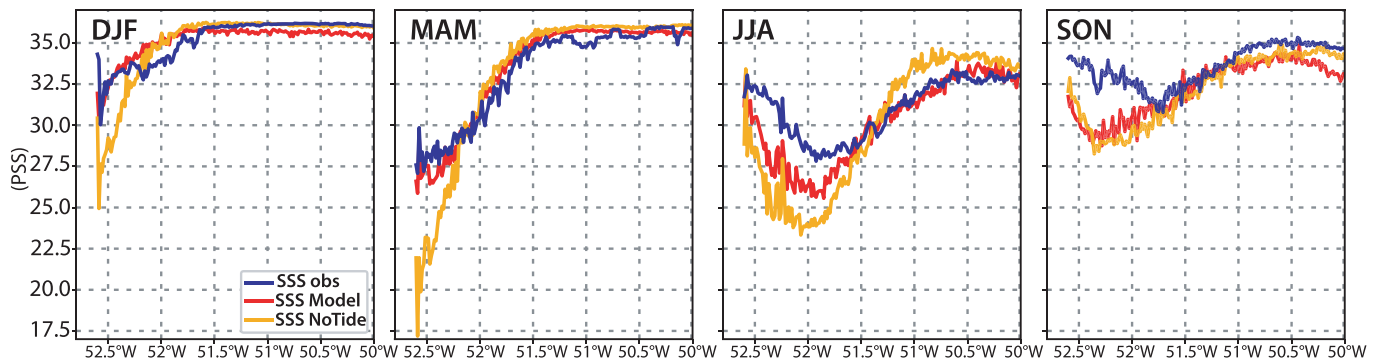


Figure 4. Observed (blue) and modeled (red for the reference simulation; yellow for the NoTide simulation) seasonal climatologies of sea surface salinity along the average ship track of Figure 2b, as a function of longitude. The coast (Kourou harbour, French Guiana) lies at 52.7°W.

performed among the numerous individual observation transects we considered, for each season. The model equivalent of these observed climatological transects (obtained by spatiotemporal interpolation of the model SSS on the gridded SSS observations) is also shown in Figure 4. It is seen that the model nicely captures the fine-scale structure of the plume, for both the position and magnitude of the fresh core, regardless of the season. The agreement is particularly good in DJF and MAM. In JJA, the model exhibits a 2-unit fresh bias from the coast to 52°W. This bias is also seen (and slightly increases) in SON. The reason for this fresh bias is unclear.

4. Results

4.1. Impact of Tide on the Amazon Plume Pathway

As the objective of the present study is to identify the impact of the tide on the plume water dispersal, we hereafter analyze the NoTide experiment. Figure 4 presents the resulting seasonal SSS obtained along the ship track. It is obvious that in all seasons except SON, the removal of the tidal flow significantly impairs the realism of the model SSS, particularly so in DJF and MAM. During both these periods, the absence of tides induces a fresh bias over the coastal part of the plume, encompassing the first 50 km (up to 52.3°W). In MAM, the maximum value of the fresh bias reaches 9 units, with a modeled value of 17.5 units, whereas both the observations and the reference simulation do not show values inferior to 26.5 there. The fresh bias of the NoTide experiment weakens but remains sensible in JJA (about 4 units less than observed and 1.5 units less than that in the reference experiment). In SON, the NoTide experiment shows a fresh bias similar to that of the reference experiment mentioned in section 3, suggesting that the tide has a limited impact on the plume characteristics during this season. At this stage, it appears that the tidal forcing is instrumental in the realism of the plume simulated along the Guiana ship track. The inclusion of the tide induces a marked increase of the surface salinity of the plume, in winter, spring, and summer. In fall, the impact of the tide on the plume SSS simulated is minor.

To gain insight into the spatial structure of the tidal effects on the characteristics of the Amazon plume, Figure 5 presents the maps of SSS, surface circulation, and sea surface height (SSH) for the model reference simulation (labeled “Model”) and for the NoTide experiment (labeled “NoTide”), along with their differences. As the sign of the tidal impact is consistent over most the seasonal cycle (DJF, MAM, and JJA), along the Guiana ship track (inducing a saltier plume core; see Figure 3) as well as over the rest of the Amazonian shelf (not shown), we present only long-term averages in Figure 5 for the sake of conciseness. As we shall see in the following, this will be clear enough to identify the processes responsible for the tidal effects on the plume water dispersal.

Figure 5a shows that the model plume is deflected northwestward upon entering the ocean. This is in line with the previous observational and modeling studies (Lentz & Limeburner, 1995; Nikiema et al., 2007). The northwestward plume export is consistent with the model surface circulation, flowing northwestward all over the continental shelf and slope region (Figure 5d). The flow is not homogenous, with strongest velocities of 1 m s^{-1} at the outer edge of the shelf and in the slope region. This is consistent with the known

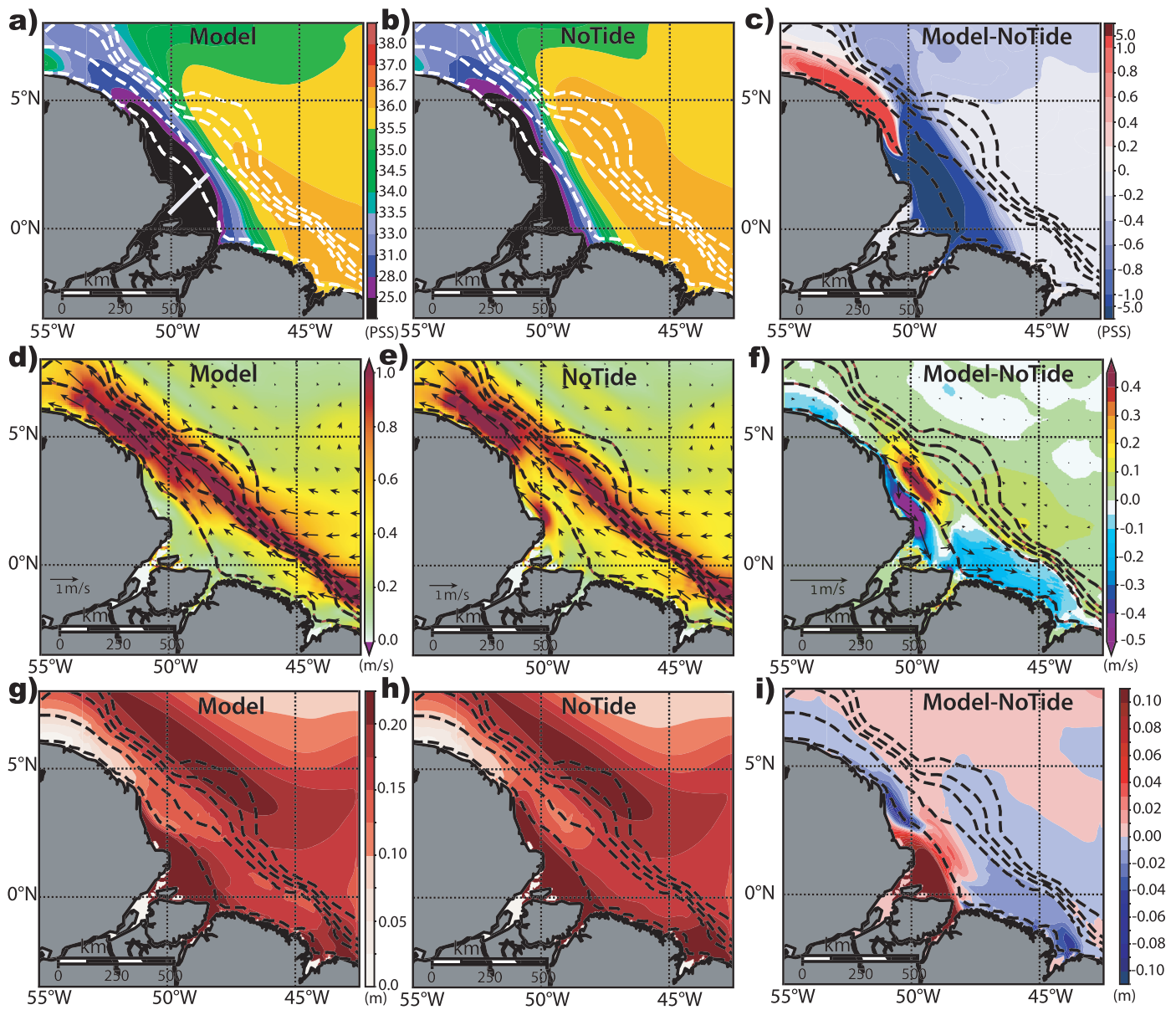


Figure 5. Long-term mean of (a–c) model SSS, (d–f) surface current, and (g–i) sea surface height. The reference simulation is in (a), (d), and (g); the NoTide simulation is in (b), (e), and (h); and their difference is in (c), (f), and (i). White solid line in (a) features the location of the section displayed on Figure 7.

pathway of the North Brazil Current (Bourlès et al., 1999; Johns et al., 1998). Weaker velocities are seen in the inner shore. However, downstream of the Amazon mouth region around Cabo Cassipore (at 5°N, 51°W; see Figure 2b), the vein of strong flow hugs the coast and remains against the coast further to the northwest. The fact that the plume propagates northwestward in the Northern Hemisphere, in the direction opposite to the propagation of coastally trapped waves, is an oddity of this river system (Lentz, 1995) and is explained by the fact that the outflow is located right at the equator (Figure 2a), where the effects of Earth rotation vanish. Ou (1989) suggested that the northwestward deflection of the plume results from the equatorial beta effect of the outflow and the local orientation of the coastline. Nikiema et al. (2007) not only partly confirmed this but also put forward the role of the ambient North Brazil Current that flows northwestward in all seasons. The model SSH (Figure 5g) suggests that the surface current flowing along the shelf break is in geostrophic balance to the north of about 3°N, with lower sea level at the coast and higher sea level around the shelf break. Equatorward of 3°N, in contrast, there is no obvious consistency between sea level isocontours and the

surface current direction, ruling out the validity of geostrophy. This result is not surprising, given the proximity of the equator. This is consistent with the observations of Lentz (1995), who concluded that northward of 3°N the Coriolis term is of the same order as the other terms of the momentum equation, in the alongshore direction. The mouth of the Amazon shows a bulge of sea level of about 25-cm height, restricted to the immediate vicinity of the river outlet.

Figure 5b shows the model SSS in the NoTide experiment. At the mouth and in the surroundings of Cabo Norte, it appears that the plume gets less extended in the offshore direction, compared to the reference simulation. In this region, the 25-unit isohaline does not extend beyond the 15-m isobath in this perturbed experiment. In the alongshore direction, in contrast, the plume extends northwestward further than in the reference simulation northwestward of Cabo Cassipore. These differences become evident in the map of the SSS differences between the two experiments (Figure 5c), with a dipolar pattern that suggests a differentiated imprint of the tide on the plume salinity: The tidal flow acts to freshen the plume everywhere, except in a narrow coastal belt originating around Cabo Cassipore (4°N, 51°W) and extending northwestward in the alongshore direction, from the coast to the shelf edge, where the salinity is inferior in the NoTide experiment. The surface circulation of the NoTide experiment appears broadly in line with that of the reference experiment, at regional scale (Figure 5e). However, locally, there are marked differences, with a swift northwestward coastal flow at Cabo Norte (as high as 0.8 m s^{-1}), whereas the flow is practically null there in the reference experiment. Conversely, offshore of this current vein, around 50°W, between the 15- and 80-m isobaths, the surface velocity is much reduced in NoTide (around 0.4 m s^{-1}) compared to 0.8 m s^{-1} in the reference experiment. These two regions of marked differences translate into a dipole of positive/negative flow velocity difference in Figure 5f. Additional sensitivity experiments without the Amazon outflow do not show this pattern (EXPA and EXPB; Figure 6), irrespective of the inclusion of tidal forcing. So the existence of the coastal jet at Cabo Norte in the NoTide experiment is bound to the existence of Amazon discharge. The stronger northwestward flow in the reference simulation around 50°W, 4°N (seen in red shade in Figure 5f), just north of the vein of weaker flow (seen in purple shade in Figure 5f), corresponds to the front of SSH difference seen there in Figure 5i and suggests it is in geostrophic balance. This front in SSH difference corresponds with the front in SSS difference seen there in Figure 5c. These three concomitant patterns together suggest that the shift in the position of the plume front between the two simulations in the cross-shore direction induces a shift in SSH that yields a geostrophically balanced alongshore velocity difference there, which is consistent with the findings in Lentz (1995). Another region of prominent, though milder, flow difference between the two simulations extends all over the shelf, to the east of the mouth (east of 48°W). The flow velocity difference is moderate, of order 0.1 m s^{-1} , but may have some important consequences on the Amazon plume properties.

The pattern of SSS difference between the reference simulation and the NoTide experiment shows a maximum near the river mouth. This appears qualitatively consistent with the modeling of Nikiema et al. (2007), although the proximity of their model open boundaries prevented them to conclude on this issue. Indeed, they attributed the offshoreward shift of the plume in their tidal simulation to an artifact of their open boundary conditions. It is seen that although the strongest differences of SSS between the two simulations are located in the coastal domain, fairly strong differences (above 0.2 unit) are also seen in the offshore ocean, north of 5°N (Figure 5c). These differences remain sensible beyond the domain of the inner model, up to 15°N (not shown). Sensible SSS differences between the two simulations are also seen to the east of the mouth, up to 47°W. The reference simulation is fresher than the NoTide experiment. Overall, the tide appears to induce a weakening of the northwestward alongshore shelf current located upstream of the freshwater plume (see section 5 for a physical explanation of this sensitivity), in such a way that may contribute to an accumulation of the freshwater plume close to the mouth. Instead, when the tidal effect on the mean circulation is absent (NoTide experiment), the plume is more easily flushed northwestward on the shelf. At this stage, our model also suggests that the prominent effect of the tidal flow is to favor the offshore export of the plume waters out of the Amazon shelf, far from the coast of North Brazil and French Guiana. In the next section, we discuss the kinematics and dynamics of these effects.

4.2. Impact of Tide on the Ocean Kinematics

Figure 7 presents the vertical sections of salinity and horizontal velocity for the reference simulation and for the NoTide perturbed simulation, in the vicinity of the Amazon River mouth. It is seen that

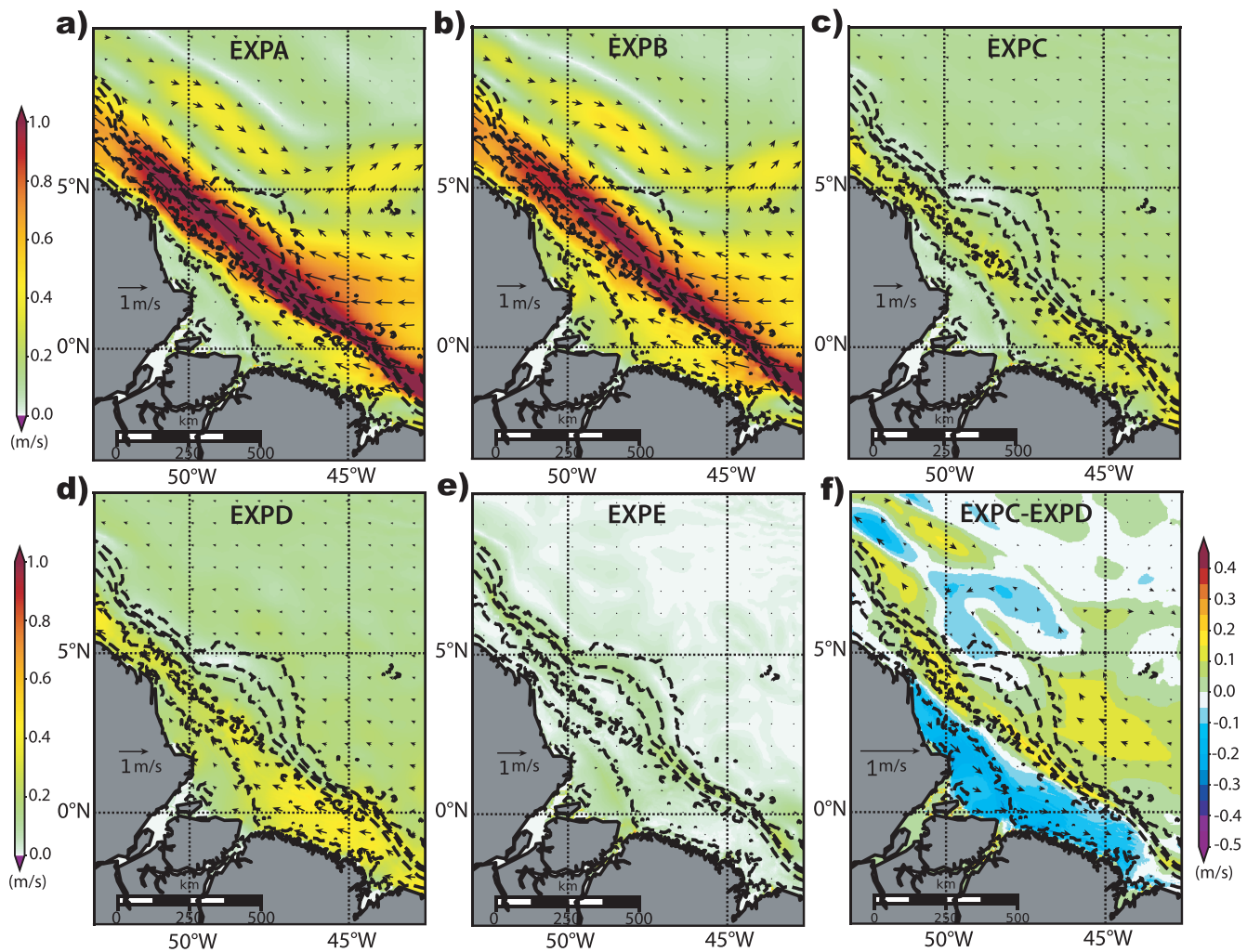


Figure 6. Surface current averaged over year 2015 for (a to e) the various model sensitivity experiments listed in Table 1, and for (f) the difference between EXPC and EXPD. Note the different color code for (f).

in the reference simulation, the plume extends from the surface down to the bottom throughout the shelf and starts shoaling under the form of a salt wedge, offshoreward of the 10-m isobath, north of 1.5°N (Figure 7a). This structure is consistent with the observations of Lentz and Limeburner (1995). In the region of the salt wedge, where the plume bottom is separated from the underlying ocean waters by a sharp halocline at around 7-m depth, the cross-shore surface flow is relatively strong toward offshore, around 0.4 m s^{-1} (Figure 7c). There, the alongshore northwestward surface flow is also the strongest, with peak values over 0.5 m s^{-1} . Shoreward of this location, the cross-shore flow remains offshoreward but weaker (0.05 to 0.1 m s^{-1}). In the NoTide simulation, in contrast, the offshoreward (due northeast) and alongshore (due northwest) flow is not barotropic on the shelf but rather surface-intensified, consistent with a salt wedge structure originating from the river mouth itself (Figure 7b). As a result, a strong halocline is seen all over the shelf, north of 0.9°N: The salinity stratification as seen in the reference simulation is shifted shoreward, in the absence of tidal forcing. It is observed that the velocity pattern of the reference simulation has also been shifted shoreward in the NoTide simulation, with the cores of strong offshoreward and alongshore northwestward flow corresponding to the location of strong salinity stratification, between 0.9°N and 1.2°N (Figure 7d). As a result, it appears that in both experiments, there is a spatial concomitance with the location of strongest salinity stratification and strongest northwestward alongshore surface

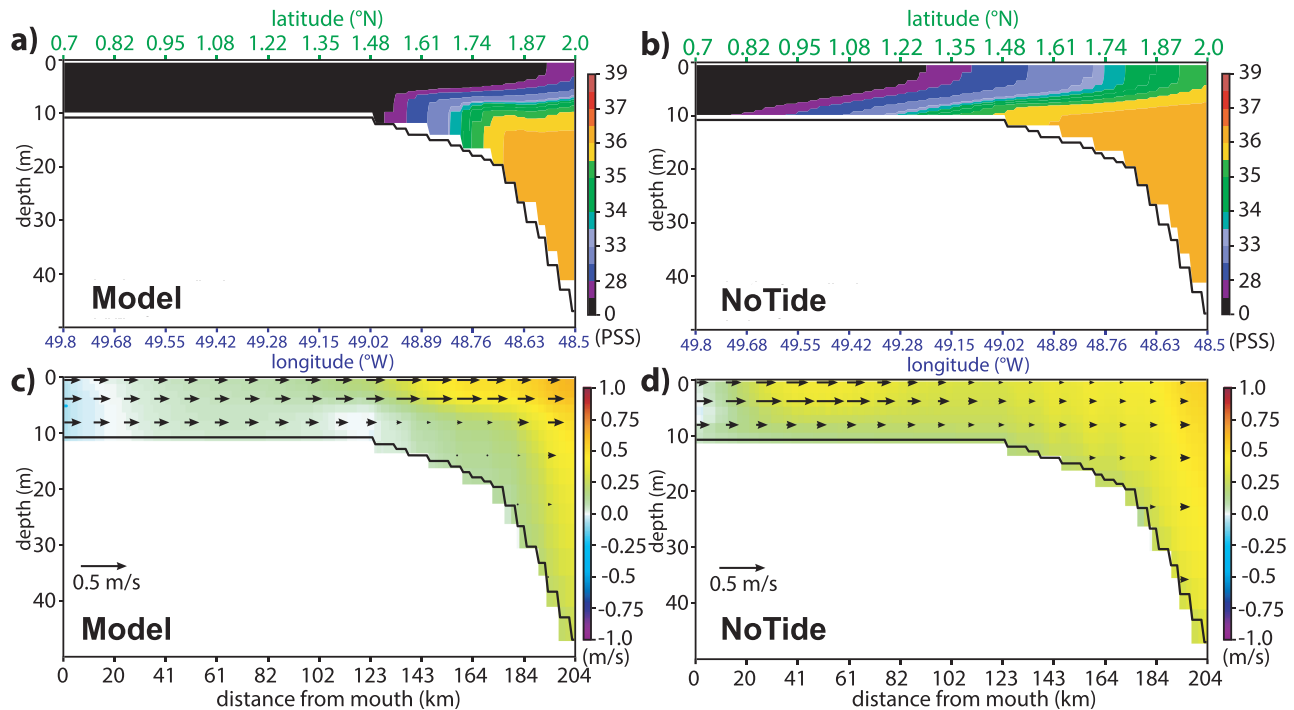


Figure 7. Vertical sections of model long-term mean (a, b) salinity and (c, d) current along the northeastward cross-shore section featured in Figure 5a. (a, c) The reference simulation, and (b, d) the NoTide experiment. For current (a, b), the arrows show the along-track/cross-shore component, and the shading shows the cross-track/alongshore component (positive northwestward).

velocity. This core sits in the slope region in the reference simulation, whereas it is shifted 150 km shoreward, in the vicinity of the river mouth, in the absence of tidal forcing. This finding is consistent with the observations reported by Geyer et al. (1991), which indicate a strong offshore surface flow only in the area of the salt wedge. In the case of the NoTide experiment, the offshore flow is consistent with the models of Nikiema et al. (2007) and Fontes et al. (2008), for their cases forced only with Amazon River discharge. We checked that we get an impact of the Amazon outflow on the cross-shore velocity similar to theirs, by carrying out sensitivity experiments without runoff forcing (EXPA and EXPB; Figures 6a and 6b). This points toward the baroclinic pressure gradient associated with the density gradient in the cross-shore direction as the dominant forcing factor of this offshoreward current. This result is in line with the observational conclusions of Lentz (1995). In the alongshore direction, Lentz (1995) suggested that the variability of the surface flow is essentially driven by the variability of the alongshore wind stress. Offshoreward of the location where the base of the plume detaches from the bottom, its thickness remains around 7 m over about 30 km and gets thinner further offshore (Figure 7a). This structure is consistent with the observations of Lentz and Limeburner (1995). On account of this thinness, these authors argued that a moderate variability of the alongshore wind stress can induce a significant variability of the alongshore surface flow. Be reminded that the alongshore component of the wind stress is prominently northwestward in all seasons (stronger during summer and weaker during winter) (Figure 1c).

Barotropic experiments (EXPC, EXPD, and EXPE; Figures 6c–6e) show that the tide, and not the density stratification, controls the magnitude of the wind-driven northwestward currents in the equatorial fraction of the shelf (3°S to 3°N). Indeed, we verified that the shelf currents in the barotropic simulations (EXPC and EXPD) are rather close to the currents in the baroclinic reference configuration, shoreward of the 80-m isobath. Moreover, the response to tidal forcing in the barotropic case (Figure 6f) is very similar to the response in the baroclinic case (Figure 5f), with a strong slowdown of the northwestward flow on the shelf in the presence of the tide. Such a sensitivity cannot be explained by a direct contribution from residual tidal currents, as EXPE shows that the residual tidal current is very weak on the shelf (Figure 6e).

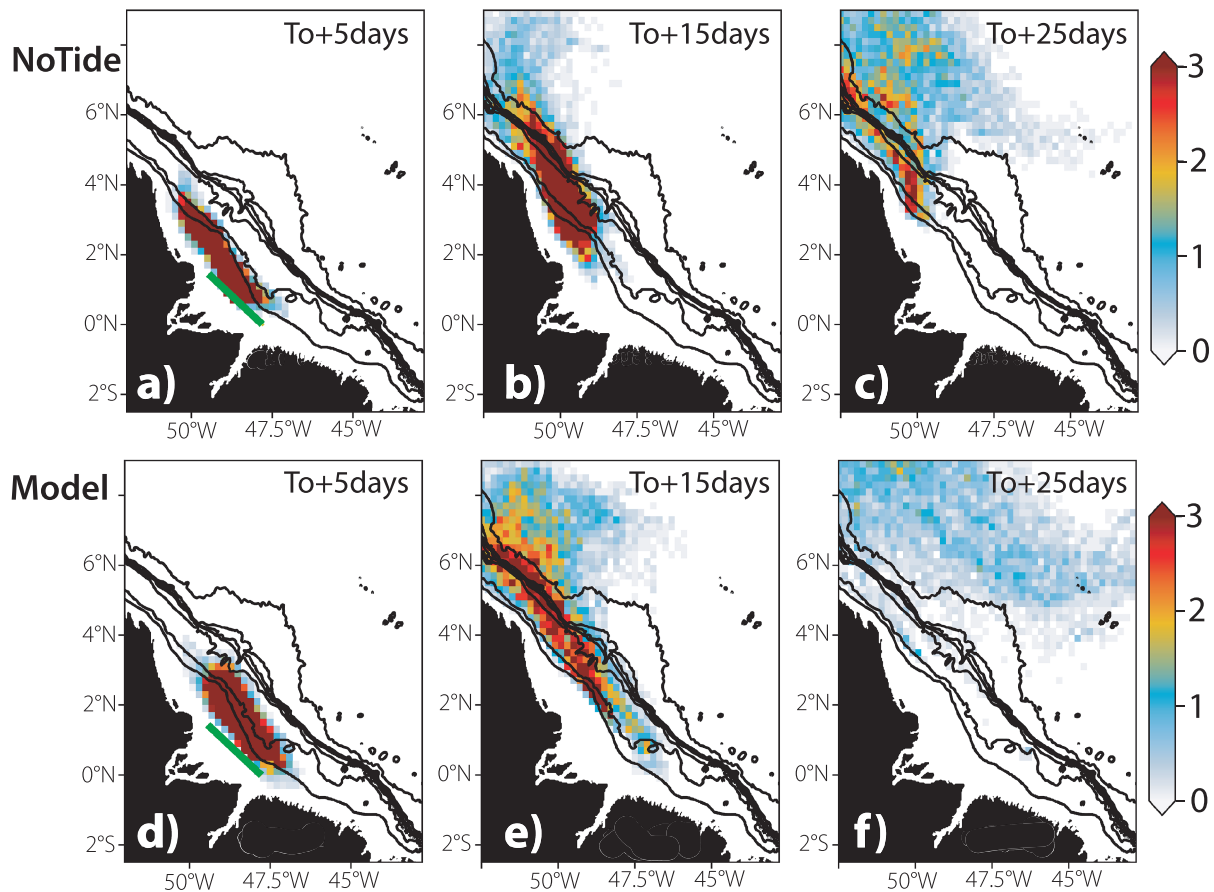


Figure 8. Evolution of the density of synthetic Lagrangian particles released in the model along the green line at 5 m depth. (a–c) for the NoTide experiment and (d–f) for the reference simulation. The spatial density of particles (a, d) after 5 days of drift, (b, e) after 15 days, and (c, f) after 25 days is shown in color. The parcels of water are released every day from years 2012 to 2015. The number of water parcels is then counted by bins of $0.1^\circ \times 0.1^\circ$ and is shown as a per-mil fraction of the total number of water parcels. A total of 15,000 water parcels were released.

5. Discussion

The response of the Amazon plume to the tidal forcing can be explained as follows. In the tidal case, there is efficient mixing on the shelf, so the momentum imparted by the wind at the surface is much efficiently transferred downward and balanced by bottom friction. Instead, weak mixing and strong stratification in the non-tidal case favor a trapping of the momentum imparted by the wind in the upper layer, which increases the transport on the shelf. These simple dynamics explain why in the absence of tidal forcing, the northwestward alongshore flow is larger than that in the reference experiment. As a result, in the absence of tidal forcing, the plume waters are deflected northwestward right after they enter the ocean and progress away from the mouth region, hugging the shoreline. They do not escape the nearshore domain. In contrast, in the reference simulation, where the tidal forcing is activated, the tidal mixing is such that the northwestward alongshore flow is weak and makes the plume waters start being deflected once they are further offshore, closer to the vein of the North Brazil Current. Besides initiating their northwestward march further offshore, they are also likely to be exposed to stronger horizontal turbulence there. Both factors act to favor the offshore export of the plume waters while they progress northwestward, which results in the larger offshore extent of the low-salinity pattern in the reference simulation (Figures 5a–5c).

The model kinematics of the reference simulation appears consistent with the AMASSEDS Lagrangian drifters analyzed by Limeburner et al. (1995): All drifters that they released in the vicinity of the Amazon mouth got exported far offshore while passing past Cabo Cassipore (traveling typically at least 50 km offshore), where our reference simulation shows a strong northwestward flow; none of the floats seem to have

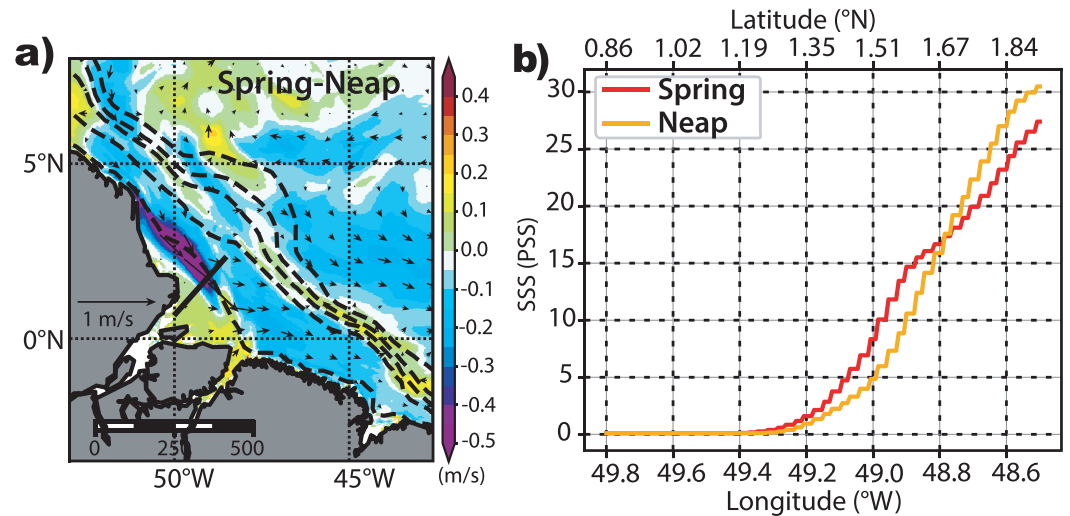


Figure 9. (a) Difference of surface current between the spring tide composite and the neap tide composite in the model. (b) Corresponding composites of SSS along the section displayed with the solid line on (a), for spring tide (red) and for neap tide (yellow).

flown through the coastal vein hugging Cabo Norte (1.5°N, 50°W) of the NoTide simulation, which suggests that such a coastally trapped vein is not realistic. The export of the Lagrangian floats through a pathway originating rather far offshore allows them to get trapped in the anticyclonic instabilities of the North Brazil Current, which pushes them further offshore, eventually—for some of them—carrying them into the North Brazil Current retroflection toward the center of the basin. We confirmed this hypothesis in our model by performing a Lagrangian tracking of synthetic particles in our model surface current, both for the reference simulation and for the NoTide case. We seeded the particles continuously across the 2012–2015 period, just offshore of the Amazon mouth, at 5 m depth (representative of the depth of the core of the river plume), and let them drift for 25 days. Our results show that the offshore export of the Lagrangian drifters, northeastward of 6°N, 50°W, is more prominent in the reference simulation than in the NoTide experiment, after 15 days of drift, and even more so after 25 days (Figure 8).

Our two extreme cases (tidal vs. nontidal ocean) can be put in parallel with the two opposed cases observed in the AMASSEDS cruises, during spring and neap tides (Beardsley et al., 1995; Geyer, 1995; Geyer & Kineke, 1995; Lentz & Limeburner, 1995) as well as in the AMANDES moorings (Prestes et al., 2018), and simulated in the idealized model of Fontes et al. (2008): According to these studies, during spring tides the production of vertical turbulence is strong enough to push offshore the location of the northwestward deflection of the plume waters, whereas during neap tides the system behaves virtually like in our NoTide experiment, with a plume being deflected northwestward right upon entering the ocean and subsequently remaining much closer to the shore. We verified this by compositing the currents and SSS of our Model experiment, during the spring tides as well as during the neap tides, over 1 year (2015). For each lunar month, we considered the 3-day periods centered on the high tide of spring tides, and averaged the 12 events to get our spring tide composite; we did the same for our neap tide composite, by considering the 3-day periods centered on the high tide of neap tides. The resulting difference of surface current is displayed in Figure 9a. It is seen that in line with our NoTide experiment, the flow during spring tides is significantly slower in the alongshore direction, in the coastal region located between Cabo Norte and Cabo Cassipore. Associated with this reduced northwestward jet in spring tide conditions, the offshore front of the freshwater plume is located further offshore and is more diffuse on the horizontal (Figure 9b). This finding is in good agreement with the observed patterns of Geyer (1995) (see his Figure 8).

6. Conclusion

This study investigates the dynamical response of the Amazon plume waters to the forcing of the tidal flow. It is found that the effect of the tidal flow is not direct: The tidal flow triggers vertical mixing of the whole

water column in the area of the Amazon River mouth, through stratified-shear flow instability. In turn, this mixed plume precludes a strong northwestward alongshore flow to set up close to the shore, allowing the plume waters to further progress offshoreward before being deflected northwestward. Unexpectedly, this influence of the tide revealed at the mouth of the Amazon River is apparently far reaching, included in the deep-ocean region, where the tidal effects on the surface stratification are expected to be negligible. It appears that the tidal effects induce a shift of dynamical regime of the plume dispersal at its source, which gives rise to a divergent evolution, with (i) a weakening of the mean currents on the shallowest fraction of the Amazon shelf that may explain the lower salinities and largest eastward extent of the plume near the mouth (between 0°N and 3°N, between 47°W and 50°W) and (ii) a prominent offshore export of the plume freshwater along its northwestward progression along the northern coast of South America. This results in a sensible effect, all the way through the North Brazil Current pathway, eventually seen in the region of its retroflexion toward the central tropical Atlantic basin. Without tidal influence, the plume waters basically hug the coast of South America, with weaker offshore export.

Given the current controversy about the possible role of ocean salinity stratification on air-sea interactions there (Grotsky et al., 2012; Hernandez et al., 2016; Jahfer et al., 2017; Newinger & Toumi, 2015; Reul et al., 2014), and keeping in mind that our reference experiment is significantly more realistic than our NoTide experiment in terms of SSS (see section 3), our study calls for a careful consideration of the ocean tide in future modeling studies of air-sea coupled dynamics in this region. As for numerical modeling of the ocean, nowadays, the scientific community, and in particular the operational oceanography agencies, is not yet in a position to explicitly account for the effects of the tide in state-of-the-art operational systems, although this is one of the targets for the next generation of operational models (Arbic et al., 2018). Our study highlights the finding that the tide is indeed an important constituent of the general circulation of the western tropical Atlantic.

Our study bears some limitations, resulting from our modeling framework. First, it has been reported that the concentration of sediments at the mouth of Amazon can be high enough to significantly influence the seawater density stratification, the horizontal and vertical pressure gradients, and thus the velocity structure. Geyer (1995) suggested that the vertical gradient of suspended sediment concentration observed in the vicinity of the river mouth can limit the intensity of the vertical turbulence. This effect, which potentially limits the efficiency of the tidally induced vertical mixing of the plume waters through the halocline, is not accounted for in our model and warrants further investigation. Indeed, because of this sediment load in the bottom layer, the actual picture may sit somewhere in between the two extreme cases of tidal and nontidal clear-water ocean we analyzed in the present study. Second, for a robust modeling of the regions under freshwater influence, where vertical mixing is known to play a key role in the freshwater budget, it has been emphasized that a high horizontal resolution (typically hectometric) is needed (Kärnä et al., 2015). Similarly, it is also known that the detailed features of the simulated river plume can depend quite strongly on the choice of the numerical schemes for subgrid parameterization of the vertical mixing of momentum and tracers (Li et al., 2005). It will be useful to check the validity of the results reported in the present study, with models with enhanced horizontal resolution and with different vertical turbulent closures. It would also be useful to investigate the effect of the high frequency variability of the tidal flow (typically the ebb-flood cycle) on the characteristics of the river plume.

Acknowledgments

Acknowledgements This research has been supported by the Gulf of Mexico Research Consortium (CIGoM), funded by the National Council of Science and Technology of Mexico—Secretariat of Energy—Hydrocarbons Trust, project 201441. J. C. was supported by Mercator Ocean International. F. D. was hosted by LIENSs/Université de La Rochelle during this work. Supercomputing facilities were provided by GENCI project GEN7298. Adrien Paris and Fabrice Papa provided insights on the hydrology of the Amazonian region. Gaël Alory provided SO SSS thermosalinograph data, and we acknowledge insight from Elodie Kestenare on the analysis of the data. V. R. performed the analysis and the figures, J. J. designed the study and performed the simulations, F. D. participated to the analysis and wrote the manuscript, J. C. and R. B. helped with the embedded numerical setup. Model results can be reproduced by using the ocean code `dev_r7963_nemo_v3_6_AGRIF-3_AGRIFVVL` (<http://forge.ipsl.jussieu.fr/nemo/wiki/Users>). The DFS5.2 forcing set is available on the server <http://servdap.legi.grenoble-inp.fr/meom/DFS5.2/>. We acknowledge the use of ARIANE software (<http://stockage.univ-brest.fr/~grima/Ariane/>) for the Lagrangian tracking experiments displayed in Figure 8.

References

- Alroy, G., Delcroix, T., Téchiné, P., Diverrès, D., Varillon, D., Cravatte, S., et al. (2015). The French contribution to the voluntary observing ships network of sea surface salinity. *Deep Sea Research Part I: Oceanographic Research Papers*, 105, 1–18. <https://doi.org/10.1016/j.dsr.2015.08.005>
- Arbic, B., Alford, M. H., Ansong, J. K., Buijsman, M. C., Ciotti, R. B., Farrar, J. T., et al. (2018). A primer on global internal tide and internal gravity wave continuum modeling in HYCOM and MITgcm. In E. Chassignet, A. Pascual, J. Tintoré, & J. Verron (Eds.), *New frontiers in operational oceanography*, (pp. 307–392). GODAE OceanView. <https://doi.org/10.17125/gov2018.ch13>
- Beardsley, R. C., Candela, J., Limeburner, R., Geyer, W. R., Lentz, S. J., Castro, B. M., et al. (1995). The M2 tide on the Amazon Shelf. *Journal of Geophysical Research*, 100(C2), 2283–2319. <https://doi.org/10.1029/94JC01688>
- Blayo, E., & Debreu, L. (1999). Adaptive mesh refinement for finite-difference ocean models: First experiments. *Journal of Physical Oceanography*, 29, 1239–1250.
- Bourlès, B., Molinari, R. L., Johns, E., & Wilson, W. D. (1999). Upper layer currents in the western tropical North Atlantic (1989–1991). *Journal of Geophysical Research*, 104(C1), 1361–1375.

- Carrère, L., F. Lyard, M. Cancet, A. Guillot, and L. Roblou (2012). FES2012: A new global tidal model taking advantage of nearly 20 years of altimetry. Paper presented at the Symposium 20 Years of Progress in Radar Altimetry, Venice, Italy.
- Coles, V. J., Brooks, M. T., Hopkins, J., Stukel, M. R., Yager, P. L., & Hood, R. R. (2013). The pathways and properties of the Amazon River plume in the tropical North Atlantic Ocean. *Journal of Geophysical Research: Oceans*, *118*, 6894–6913. <https://doi.org/10.1002/2013JC008981>
- Dai, A., & Trenberth, K. E. (2002). Estimates of freshwater discharge from continents: Latitudinal and seasonal variations. *Journal of Hydrometeorology*, *3*, 660–687.
- Debreu, L. (2000). Raffinement adaptatif de maillage et méthode de zoom. Application aux modes d'océan. Ph.D. Thesis, Université Joseph Fourier, Grenoble, France.
- Dee, D. P., Uppala, S. M., Simmons, A. J., Berrisford, P., Poli, P., Kobayashi, S., et al. (2011). The ERA-Interim reanalysis: Configuration and performance of the data assimilation system. *Quarterly Journal of the Royal Meteorological Society*, *137*(656), 553–597. <https://doi.org/10.1002/qj.828>
- Durand, F., Piecuch, C., Becker, M., Papa, F., Sherin, V. R., Khan, J. U., & Ponte, R. (2019). Impact of continental freshwater runoff on coastal sea level. *Surveys in Geophysics*, *40*(6), 1437–1466. <https://doi.org/10.1007/s10712-019-09536-w>
- Dussin, R., B. Barnier, and L. Brodeau (2016). Up-dated description of the DFS5 forcing data set: The making of Drakkar forcing set DFS5, DRAKKAR/MyOcean Rep. 01-04-16, Lab. of Glaciol. and Environ. Geophys., Grenoble, France.
- Fontes, R. F. C., Castro, B. M., & Beardsley, R. C. (2008). Numerical study of circulation on the inner Amazon Shelf. *Ocean Dynamics*, *58*(3–4), 187–198. <https://doi.org/10.1007/s10236-008-0139-4>
- Fournier, S., Reager, J. T., Lee, T., Vazquez-Cuervo, J., David, C. H., & Gierach, M. M. (2016). SMAP observes flooding from land to sea: The Texas event of 2015. *Geophysical Research Letters*, *43*, 10,338–10,346. <https://doi.org/10.1002/2016GL070821>
- Fournier, S., Vialard, J., Lengaigne, M., Lee, T., Gierach, M. M., & Chaitanya, A. V. S. (2017). Modulation of the Ganges-Brahmaputra river plume by the Indian Ocean dipole and eddies inferred from satellite observations. *Journal of Geophysical Research: Oceans*, *122*, 9591–9604. <https://doi.org/10.1002/2017JC013333>
- Geyer, W. R. (1995). Tide-induced mixing in the Amazon Frontal Zone. *Journal of Geophysical Research*, *100*(C2), 2341–2353. <https://doi.org/10.1029/94JC02543>
- Geyer, W. R., Beardsley, R. C., Candela, J., Castro, B. M., Legeckis, R. V., Lentz, S. J., et al. (1991). The physical oceanography of the Amazon outflow. *Oceanography*, *4*(1), 8–14.
- Geyer, W. R., Beardsley, R. C., Lentz, J., Candela, J., Limeburner, R., Johns, W., et al. (1996). Physical oceanography of the Amazon shelf. *Continental Shelf Research*, *16*, 575–616. [https://doi.org/10.1016/0278-4343\(95\)00051-8](https://doi.org/10.1016/0278-4343(95)00051-8)
- Geyer, W. R., & Kineke, G. C. (1995). Observations of currents and water properties in the Amazon frontal zone. *Journal of Geophysical Research*, *100*(C2), 2321–2339. <https://doi.org/10.1029/94JC02657>
- Gibbs, R. J. (1970). Circulation in the Amazon River estuary and adjacent Atlantic Ocean. *Journal of Marine Research*, *28*, 113–123.
- Giffard, P., Llovel, W., Jouanno, J., Morvan, G., & Decharme, B. (2019). Contribution of the Amazon River discharge to regional sea level in the tropical Atlantic Ocean. *Water*, *11*, 2348.
- Grodsky, S. A., Reul, N., Lagerloef, G. S. E., Reverdin, G., Carton, J. A., Chapron, B., et al. (2012). Haline hurricane wake in the Amazon/Orinoco plume: AQUARIUS/SACD and SMOS observations. *Geophysical Research Letters*, *39*, L20603. <https://doi.org/10.1029/2012GL053335>
- Hernandez, O., Jouanno, J., & Durand, F. (2016). Do the Amazon and Orinoco freshwater plumes really matter for hurricane-induced ocean surface cooling? *Journal of Geophysical Research: Oceans*, *121*, 2119–2141. <https://doi.org/10.1002/2015JC011021>
- Hernandez, O., Jouanno, J., Echevin, V., & Aumont, O. (2017). Modification of sea surface temperature by chlorophyll concentration in the Atlantic upwelling systems. *Journal of Geophysical Research: Oceans*, *122*, 5367–5389. <https://doi.org/10.1002/2016JC012330>
- Horner-Devine, A. R., Hetland, R. D., & MacDonald, D. G. (2015). Mixing and transport in coastal river plumes. *Annual Review of Fluid Mechanics*, *47*(1), 569–594. <https://doi.org/10.1146/annurev-fluid-010313-141408>
- HYBAM (2018). Contrôles géodynamique, hydrologique et biogéochimique de l'érosion/altération et des transferts de matière dans les bassins de l'Amazone, de l'Orénoque et du Congo. [Available at <http://www.ore-hybam.org>. last accessed 29 November 2018]
- Jahfer, S., Vinayachandran, P. N., & Nanjundiah, R. S. (2017). Long-term impact of Amazon River runoff on northern hemispheric climate. *Scientific Reports*, *7*, 1–9.
- Johns, W. E., Lee, T. N., Beardsley, R. C., Candela, J., Limeburner, R., & Castro, B. (1998). Annual cycle and variability of the North Brazil Current. *Journal of Physical Oceanography*, *28*, 103–128.
- Kärnä, T., Baptista, A. M., Lopez, J. E., Turner, P. J., McNeil, C., & Sanford, T. B. (2015). Numerical modeling of circulation in high-energy estuaries: A Columbia River estuary benchmark. *Ocean Modelling*, *88*, 54–71. <https://doi.org/10.1016/j.ocemod.2015.01.001>
- Le Bars, Y., Lyard, F., Jeandel, C., & Dardengo, L. (2010). The AMANDES tidal model for the Amazon estuary and shelf. *Ocean Modelling*, *31*(3–4), 132–149. <https://doi.org/10.1016/j.ocemod.2009.11.001>
- Lentz, S. J. (1995). The Amazon River plume during AMASSEDS: Subtidal current variability and the importance of wind forcing. *Journal of Geophysical Research*, *100*(C2), 2377–2390. <https://doi.org/10.1029/94JC00343>
- Lentz, S. J., & Limeburner, R. (1995). The Amazon River plume during AMASSEDS: Spatial characteristics and salinity variability. *Journal of Geophysical Research*, *100*(C2), 2355. <https://doi.org/10.1029/94jc01411>
- Li, M., Zhong, L., & Boicourt, W. C. (2005). Simulations of Chesapeake Bay estuary: Sensitivity to turbulence mixing parameterizations and comparison with observations. *Journal of Geophysical Research*, *110*, C12004. <https://doi.org/10.1029/2004JC002585>
- Limeburner, R., Beardsley, R. C., Soares, I. D., Lentz, S. J., & Candela, J. (1995). Lagrangian flow observations of the Amazon River discharge into the North Atlantic. *Journal of Geophysical Research*, *100*(C2), 2401–2415. <https://doi.org/10.1029/94JC03223>
- Madec, G. (2014). “NEMO ocean engine” (Draft edition r5171), Note du Pôle de modélisation 27, Inst. Pierre-Simon Laplace, France, ISSN No 1288-1619.
- Maraldi, C., Chanut, J., Levier, B., Ayoub, N., de Mey, P., Refray, G., et al., & the Mercator Research and Development Team (2013). NEMO on the shelf: Assessment of the Iberia-Biscay-Ireland configuration. *Ocean Science*, *9*(4), 745–771. <https://doi.org/10.5194/os-9-745-2013>
- Newinger, C., & Toumi, R. (2015). Potential impact of the colored Amazon and Orinoco plume on tropical cyclone intensity. *Journal of Geophysical Research: Oceans*, *120*, 1296–1317. <https://doi.org/10.1002/2014JC010533>
- Nikiema, O., Devenon, J.-L., & Baklouti, M. (2007). Numerical modeling of the Amazon River plume. *Continental Shelf Research*, *27*(7), 873–899.
- Ou, H. W. (1989). Why does the Amazon water flow to the North after its discharge? *Journal of Physical Oceanography*, *19*, 1102–1107.

- Paluszkiwicz, T., Curtin, T. B., & Chao, S.-Y. (1995). Wind-driven variability of the Amazon River plume on the continental shelf during the peak season. *Geo-Marine Letters*, *15*, 179–184.
- Prestes, Y. O., da Silva, A. C., & Jeandel, C. (2018). Amazon water lenses and the influence of the North Brazil Current on the continental shelf. *Continental Shelf Research*, *160*, 36–48. <https://doi.org/10.1016/j.csr.2018.04.002>
- Reul, N., Quilfen, Y., Chapron, B., Fournier, S., Kudryavtsev, V., & Sabia, R. (2014). Multisensor observations of the Amazon-Orinoco river plume interactions with hurricanes. *Journal of Geophysical Research: Oceans*, *119*, 8271–8295. <https://doi.org/10.1002/2014JC010107>
- Silva, C. E., & Castelao, R. M. (2018). Mississippi River plume variability in the Gulf of Mexico from SMAP and MODIS-Aqua observations. *Journal of Geophysical Research: Oceans*, *123*, 6620–6638. <https://doi.org/10.1029/2018JC014159>
- Simpson, J. H. (1997). Physical processes in the ROFI regime. *Journal of Marine Systems*, *12*(1-4), 3–15. [https://doi.org/10.1016/s0924-7963\(96\)00085-1](https://doi.org/10.1016/s0924-7963(96)00085-1)
- Weatherall, P., Marks, K. M., Jakobsson, M., Schmitt, T., Tani, S., Arndt, J. E., et al. (2015). A new digital bathymetric model of the world's oceans. *Earth and Space Science*, *2*, 331–345.
- Wu, H., Shen, J., Zhu, J., Zhang, J., & Li, L. (2014). Characteristics of the Changjiang plume and its extension along the Jiangsu Coast. *Continental Shelf Research*, *76*, 108–123. <https://doi.org/10.1016/j.csr.2014.01.007>
- Wu, H., Zhu, J., Shen, J., & Wang, H. (2011). Tidal modulation on the Changjiang River plume in summer. *Journal of Geophysical Research*, *116*, C08017. <https://doi.org/10.1029/2011JC007209>